Monthly Notices
of the
ROYAL ASTRONOMICAL SOCIETY

Mon. Not. R. Astron. Soc. **422,** 968–980 (2012) doi:10.1111/j.1365-2966.2012.20643.x

CO depletion in the Gould Belt clouds

H. Christie,[1⋆] S. Viti,[1] J. Yates,[1] J. Hatchell,[2] G. A. Fuller,[3] A. Duarte-Cabral,[4,5] S. Sadavoy,[6] J. V. Buckle,[7,8] S. Graves,[7,8] J. Roberts,[9] D. Nutter,[10] C. Davis,[11] G. J. White,[12,13] M. Hogerheijde,[14] D. Ward-Thompson,[10] H. Butner,[15] J. Richer[7,8] and J. Di Francesco[16]

[1]*Department of Physics and Astronomy, UCL, Gower Street, London WC1E 6BT*
[2]*School of Physics, University of Exeter, Stocker Road, Exeter EX4 4QL*
[3]*Jodrell Bank Centre for Astrophysics, School of Physics and Astronomy, University of Manchester, Oxford Road, Manchester M13 9PL*
[4]*Univ. Bordeaux, LAB, UMR 5804, F-33270 Floriac, France*
[5]*CNRS, LAB, UMR 5804, F-33270 Floriac, France*
[6]*Department of Physics and Astronomy, University of Victoria, PO Box 355, STN CSC, Victoria, BC V8W 3P6, Canada*
[7]*Astrophysics Group, Cavandish Laboratory, JJ Thomson Avenue, Cambridge CB3 0HE*
[8]*Kavli Institute for Cosmology, c/o Institute of Astronomy, University of Cambridge, Madingley Road, Cambridge CB3 0HA*
[9]*Instituto Nacional de Technica Aeroespacial, 28830 San Fernando de Henares, Spain*
[10]*School of Physics and Astronomy, Cardiff University, Queen's Buildings, The Parade, Cardiff CF24 3AA*
[11]*Joint Astronomy Centre, 660 North A'ohoku Place, University Park, Hilo, HI 96720, USA*
[12]*Department of Physics and Astronomy, The Open University, Milton Keynes MK7 6AA*
[13]*The Rutherford Appleton Laboratory, Space Science and Technology Division, Didcot OX11 0NL*
[14]*Leiden Observatory, Leiden University, PO Box 9513, 2300 RA Leiden, the Netherlands*
[15]*Department of Physics and Astronomy, James Madison University, Harrisonburg, VA 22807, USA*
[16]*National Research Council of Canada, Herzberg Institute of Astrophysics, Department of Physics and Astronomy, University of Victoria, Victoria, BC V9E 2E7, Canada*

Accepted 2012 January 27. Received 2012 January 26; in original form 2011 November 18

ABSTRACT

We present a statistical comparison of CO depletion in a set of local molecular clouds within the Gould Belt using Sub-millimetre Common User Bolometer Array (SCUBA) and Heterodyne Array Receiver Programme (HARP) data. This is the most wide-ranging study of depletion thus far within the Gould Belt. We estimate CO column densities assuming local thermodynamic equilibrium and, for a selection of sources, using the radiative transfer code RADEX in order to compare the two column density estimation methods. High levels of depletion are seen in the centres of several dust cores in all the clouds. We find that in the gas surrounding protostars, levels of depletion are somewhat lower than for starless cores with the exception of a few highly depleted protostellar cores in Serpens and NGC 2024. There is a tentative correlation between core mass and core depletion, particularly in Taurus and Serpens. Taurus has, on average, the highest levels of depletion. Ophiuchus has low average levels of depletion which could perhaps be related to the anomalous dust grain size distribution observed in this cloud. High levels of depletion are often seen around the edges of regions of optical emission (Orion) or in more evolved or less dynamic regions such as the bowl of L1495 in Taurus and the north-western region of Serpens.

Key words: molecular data – stars: abundances – stars: formation – ISM: abundances.

1 INTRODUCTION

In dense, cold, star-forming cores, molecules in the gas phase freeze-out on to dust grains, forming icy mantles on grain surfaces. The extent to which this freeze-out (or depletion) occurs for a particular molecule depends on a complicated chemistry that varies non-linearly with time and physical environment. The strong dependence of depletion on the age and make-up of a core could make it a useful probe of core history.

Depletion is difficult to quantify observationally. It is common to use gas phase emission from molecules such as CO to infer the fraction of the species that is in the solid phase. This requires a comparison of gas phase molecular line emission with continuum emission from dust. Several assumptions are made about the state of the emitting gas and dust, and the possible destruction of the

⋆E-mail: hc@star.ucl.ac.uk

molecule by other means is often ignored. This method has been successful, and studies show significant depletion in star forming cores (see Caselli et al. 1999; Bacmann et al. 2002; Redman et al. 2002; Savva et al. 2003; Thomas & Fuller 2008; Duarte-Cabral et al. 2010).

In addition to studies of the gas phase, one can directly observe molecules in the solid state using e.g. the absorption of IR emission from background sources (see reviews by van Dishoeck 2004; Öberg et al. 2011).

Several authors have attempted to model cores including freeze-out reactions to replicate observed line strengths and profiles. These models require accurate depletion and desorption rate estimates from laboratory experiments that are very difficult to make. Desorption can occur as a result of several processes including direct impact of cosmic rays which cause local heating of the grain surface, leading to the desorption of species in the mantle. Cosmic rays will also ionize or excite molecules as they pass through the dense gas in a molecular core. UV photons are produced as a result of these excitations and these, in turn, can impart energy to the grain surface by dissociation of molecules in the mantle (particularly water). The formation of hydrogen molecules on grains will also cause local heating of the surface. The relative importance of these as desorption mechanisms in the dark cloud environment is discussed in Roberts et al. (2007). It is worth noting that, despite recent experiments (Öberg et al. 2009; Muñoz Caro et al. 2010), rates of non-thermal desorption as a function of density and mantle composition, required for chemical codes, have not yet been accurately determined. Even with these uncertainties, modelling provides strong arguments for depletion of molecules in dense cores. In many cases where multiple observations of different species are available, it is impossible to reproduce observationally derived abundances and ratios between abundances without substantial freeze-out, suggesting that this is an important contributor to the chemistry of star-forming regions (e.g. Taylor & Williams 1996; Aikawa et al. 2001; Viti et al. 2003).

To study how the depletion of CO relates to environment, one requires line data from the CO isotopologues as well as continuum data from dust, from a variety of sources. The James Clerk Maxwell Telescope (JCMT) Gould Belt Survey (GBS; Ward-Thompson et al. 2007) can provide these data. The Gould Belt is a system of kinematically related stars and gas, mainly within 500 pc, highlighted by O- and B-type stars and containing numerous interesting and well-studied molecular clouds, all with very different properties. The GBS, making use of Sub-millimetre Common User Bolometer Array-2 (SCUBA-2) (dust continuum emission), POL-2 and Heterodyne Array Receiver Programme (HARP) (spectral line emission for three isotopologues of CO) on the JCMT, aims to achieve consistent and detailed sets of data for many star-forming regions within the Gould Belt (see Buckle et al. 2010, 2011; Davis et al. 2010; Graves et al. 2010; White et al., in preparation, for the survey first look papers). This survey will help to build a better picture of star formation and how it is linked to environment. In this paper we use the early GBS spectral data from HARP together with catalogues of dust cores collated by Sadavoy et al. (2010) from SCUBA dust emission maps to study depletion in five GBS regions, representing a range of physical conditions: NGC 2024 and NGC 2071 in Orion, L1495 in Taurus, the Ophiuchus main cloud core (L1688), and the Serpens main cluster. We compare the depletions using a consistent methodology that allows meaningful comparisons between these regions to be made. We discuss how depletion factors are calculated, compare local thermodynamic equilibrium (LTE) methods with the use of RADEX and discuss how depletion varies in a region and between regions.

2 DATA

The HARP instrument at the JCMT in Hawaii (see Buckle et al. 2009, for more details of HARP) was used to map regions in Orion, Taurus, Serpens and Ophiuchus as part of the JCMT Gould Belt Legacy Survey. Table 1 lists the sizes of and distance to each cloud as well as the centre, area and sensitivity of each respective map. In conjunction with Auto-Correlation Spectral Imaging System (ACSIS), spectra were obtained for the ^{12}CO $J = (3 \rightarrow 2)$ line at 345.796 GHz at high and low resolution. HARP used wide-band imaging (up to 1.9 GHz bandwidth) in single sideband mode to cover both the $J = (3 \rightarrow 2)$ transitions of ^{13}CO and C^{18}O at 330.588 and 329.331 GHz, respectively. Narrow-band imaging results in higher resolution spectra with channels of up to 31 kHz. ^{12}CO maps generally cover physically larger areas. The data have a spectral resolution of 0.05 km s^{-1} or 0.85 km s^{-1} for the high- and low-resolution setups, respectively. We use only the smaller sections of maps for which spectra from all three isotopologues are available and use the high-resolution images of ^{12}CO.

HARP has 16 receivers, separated by 30 arcsec in the focal plane, resulting in a footprint of around 2 arcmin projected on the sky. The beam width of the JCMT is ∼14 arcsec full width at half-maximum (FWHM) at the frequencies of the CO lines. For a fully sampled map, telescope scans were made in the raster position-switched observing mode where the telescope scans along the direction parallel to the edges of the map, taking spectra separated by 7.3 arcsec. This is done first in one direction and then again in the perpendicular direction for better coverage (the basket weave technique). Pixels thus represent regions on the sky that are around 7 arcsec apart (see Buckle et al. 2010, for more detail). Noise levels vary from map to map depending on weather conditions at the time of data acquisition and total hours dedicated to each observation. We used the current best reductions for each cloud. The resulting maps were not reduced entirely similarly but the differences in reduction techniques for the separate regions (type of binning used, etc.) have a minor effect on the results. Detailed information on the maps and their reductions can be found in the GBS first look papers (referenced in Section 1).

We use results from dust emission data produced using SCUBA, also at the JCMT, as part of the SCUBA Legacy Catalogue (Di Francesco et al. 2008). SCUBA is comprised of two hexagonal arrays of detectors, a long-wave array with 37 pixels and a short wave array with 91 pixels. The relevant data are maps of 850-μm emission taken using the long-wave array and smoothed with a 1σ Gaussian (see Di Francesco et al. 2008, for details), resulting in a spatial resolution for each Scuba Legacy Catalogue (SLC) map of 22.9 arcsec at 850 μm.

3 A DEPLETION FACTOR FOR THE DUST CORES – LTE ANALYSIS

Our sample of dust cores is taken directly from the catalogue produced by Sadavoy et al. (2010) using the SCUBA 850-μm dust emission maps mentioned above. These authors used the clump identification algorithm 'CLUMPFIND' (Williams, de Geus & Blitz 1994) to pick out localized regions of strong emission. CLUMPFIND first identifies closed contours at the highest level of emission in the map as peaks, then contours in flux down to a minimum level that is specified by the user. The area inside the minimum contour, and including a peak, is defined as the clump and integrated emission as well as peak values are outputted. We compared peak fluxes at the centre of each core from the Sadavoy et al. catalogue

Table 1. Details of the observations.

Region	Distance (pc)	Isotopologue	Map centre (J2000)	Map area (arcsec^2)	rms noise (K)[a]
Serpens	260	^{12}CO	18^h30^m $1^\circ14'$	260	0.12
		^{13}CO	18^h30^m $1^\circ13'$	77	0.24
		C^{18}O	18^h30^m $1^\circ13'$	77	0.25
Taurus	140	^{12}CO	4^h18^m 4^h20^m(se) $28^\circ22'$ $27^\circ11'$(se)	264/120(se)[b]	0.10/0.13(se)
		^{13}CO	as ^{12}CO	450/378(se)	0.15/0.24(se)
		C^{18}O	as ^{12}CO	450/378(se)	0.18/0.29(se)
Ophiuchus	125	^{12}CO	16^h28^m $-24^\circ33'$	900	0.49
		^{13}CO	as ^{12}CO	256	0.18
		C^{18}O	as ^{12}CO	256	0.16
NGC 2024	415	^{12}CO	05^h42^m $-01^\circ54'$	243	0.11
		^{13}CO	as ^{12}CO	as ^{12}CO	0.18
		C^{18}O	as ^{12}CO	as ^{12}CO	0.14
NGC 2071	415	^{12}CO	05^h47^m $00^\circ20'$	292	0.21
		^{13}CO	as ^{12}CO	as ^{12}CO	0.10
		C^{18}O	as ^{12}CO	as ^{12}CO	0.13

[a]Rms noise values in 0.1 km s^{-1} channels.
[b]The letters 'se' refer to the south-eastern region of Taurus L1495.

with our CO data at the same position. We refer to the identified regions as 'cores' since their sizes are generally less than 0.1 pc and they contain typically a few solar masses of material. A typical starless core has a density of around 10^5 cm^{-3} and temperature 10 K (Di Francesco et al. 2007). Since CO freezes out below ∼20 K (15–17 K; Nakagawa 1980), and the amount of freeze-out should directly scale with the density of the surrounding material (Rawlings et al. 1992), the high densities and low temperatures observed in the centres of these cores are expected to result in significant depletion of CO on to dust grains. Hence, we derive hydrogen column densities from both the dust and C^{18}O data and use the ratio between the two as a measure of depletion in the core centres. To this end, C^{18}O is preferred to either ^{13}CO or ^{12}CO because it is more optically thin, and thus more representative of the whole column of gas, than either of the other two isotopologues. To derive a column density from the dust emission, we assume that emission from dust arises from an opacity modulated blackbody curve at a temperature of 10 K for the starless cores and 20 K for those coincident with a young stellar object (YSO) candidate identified by *Spitzer* (i.e. the protostellar cores). We discuss the implications of assuming fixed dust temperatures for the cores in Section 6. To infer the total column density of the dust from the emission at 850 μm, we use

$$F_\nu = \int_\Omega \mathrm{B}_\nu(T, \nu)\kappa_\nu N_{\mathrm{H}_2}\mu m_\mathrm{p}\mathrm{d}\Omega \quad (1)$$

where F_ν is the peak flux per beam at frequency ν, B_ν is the blackbody function at the same frequency and temperature T, κ_ν is the dust emissivity per unit mass of gas and dust at the same frequency, N_{H_2} is the column density of molecular hydrogen, μ is the mean molecular mass, m_p is the mass of a proton and Ω is the beam size of the relevant telescope. We assume a dust emissivity of 1.97 cm^2 g^{-1} (Ossenkopf & Henning 1994), assuming grains in a gas volume density of 10^6 cm^{-3} with thin ice mantles. The same paper quotes a value for the dust emissivity with a thick ice mantle of 1.47 cm^2 g^{-1}. This represents a small error compared to, for example, temperature estimates, so we do not consider the change in optical properties of the grains due to the growth of icy mantles to be a dominant effect. The equation above assumes an emitting area larger than the beam size of the relevant telescope. The beam size of the JCMT is generally smaller than CLUMPFIND derived diameters for the dust cores, so we do not consider beam dilution effects to be a problem and assume a beam filling factor of 1 in all cases.

The hydrogen column densities from the C^{18}O maps were first derived assuming LTE and optically thin emission. Critical densities of the CO lines (some 10^4 cm^{-3}) are generally lower than the typical core density of around 10^6 cm^{-3}, so material should be thermalized. Buckle et al. (2010) calculated optical depths for the three CO isotopologue lines in Orion B and showed that the C^{18}O line is optically thin across the whole of the imaged region, so our assumption of low optical depth in the C^{18}O lines is likely to be valid even in the denser dust cores (in Section 6 we consider the implications of optical depth effects on our depletion results). Accordingly, the Boltzmann and Planck equations give

$$N(\mathrm{C}^{18}\mathrm{O}) = \frac{(5.21\times10^{12})\times T_\mathrm{ex}(^{12}\mathrm{CO})\times\int T_\mathrm{mb}\mathrm{d}v}{\mathrm{e}^{-31.6/T_\mathrm{ex}(^{12}\mathrm{CO})}}, \quad (2)$$

where N(C^{18}O) is the column density of C^{18}O (cm^{-2}), T_ex(^{12}CO) is the excitation temperature of the line (from the ^{12}CO line profile), and T_mb is the main beam temperature.

We then assumed a N(C^{18}O)/N(H$_2$) ratio of 1.7×10^{-7} (Frerking, Langer & Wilson 1982) to convert from C^{18}O to hydrogen column density. We discuss the implications of this assumption in Section 6.

We used the peak temperature of the ^{12}CO line to estimate the gas kinetic temperature, and hence the line excitation temperature in LTE, using

$$T_{\rm ex}(^{12}{\rm CO}) = \frac{16.59K}{\ln(1 + \frac{16.6}{T_{\rm max}(^{12}{\rm CO})+0.036})}, \quad (3)$$

again following from the Boltzmann and Planck equations describing LTE, assuming an optically thick line. $T_{\rm max}$ is the peak temperature of the ^{12}CO line at the centre of the dust core. We adopt a main beam efficiency of 0.63 (Buckle et al. 2009). More detail on the derivation of equation (3) can be found in Pineda, Caselli & Goodman (2008). The 0.036 term results from the removal of the cosmic microwave background at 2.7 K.

The use of equation (3) requires that the ^{12}CO line be optically thick and not self-absorbed at its peak. In the case of the ^{12}CO maps, lines are often self-absorbed and so cannot be used to estimate an accurate gas temperature in all cases. If we assume the ^{13}CO line to be optically thick, it can be used in place of the ^{12}CO line, in a modified form of equation (3), to estimate the excitation temperature in cores where the latter is obviously self-absorbed. We used the ^{13}CO line to estimate the temperature if the ^{13}CO line peak was higher than the ^{12}CO in the line centre, otherwise the ^{12}CO line was considered to be sufficiently accurate. The ^{13}CO lines, however, were also self-absorbed. In these cases, we used the peak line temperature (i.e. the height of the peaks at the line edge rather than at the centre) as the best possible first estimate of the gas temperature and note that these will probably be slightly underestimated in several cases.

It is difficult, looking at the profiles of the three lines together, to disentangle the effects of self-absorption from the possibility of there being several CO condensations lying along the line of sight. The position of the C^{18}O peak can help, but again in many cases it does not peak at the frequency where the ^{13}CO and ^{12}CO lines dip, which would definitely point to self-absorption in the latter two isotopologues. Of the 186 cores, in total roughly 60 per cent have a clear double peak in the ^{12}CO line. For 70 per cent of these, the C^{18}O line peaks in the dip of the ^{12}CO line. The rest of the profiles (making up roughly 20 per cent of the total) are more complicated with the C^{18}O line peaking nearer in frequency to one of the ^{12}CO line peaks or itself showing a double profile. For consistency, we adopted the approach detailed above, using the ^{12}CO and ^{13}CO to find a kinetic temperature, even when self-absorbed. In Section 6 we discuss the implications of using ^{12}CO and ^{13}CO, which probably trace hotter gas than the dust, to derive excitation temperatures for the central regions of the cores.

The integrated intensity of the C^{18}O emission was found by fitting a Gaussian profile to the line using DIPSO (part of the STARLINK software package; Warren-Smith & Wallace 1993). In cases where the C^{18}O exhibited two or more peaks, the separate peaks were considered to be due to distinct cores along the line of sight and we included emission from all lines in the sum. In doing this, we assume that emission from dust derives from all cores along the line of sight and we find an average measure of the depletion factor. Such cores will not, in reality, contain equal amounts of dust, but since it is not possible to disentangle the dust emission from different cores along the line of sight we are unable to estimate the level of depletion in individual cores. Using the hydrogen column density calculated from the dust data and the hydrogen column density calculated from the C^{18}O, we derived a depletion factor, $F_{\rm dep}$, given by

$$F_{\rm dep} = \frac{N({\rm H_2})_{\rm dust}}{N({\rm H_2})_{\rm CO}}, \quad (4)$$

where $N({\rm H_2})_{\rm dust}$ and $N({\rm H_2})_{\rm CO}$ are the hydrogen column densities calculated from the dust and the C^{18}O, respectively.

The more CO is depleted on to dust grains, the lower the hydrogen column density derived from the CO gas phase emission and hence the higher the value of $F_{\rm dep}$. In Section 6, we discuss the uncertainties in the derived depletion factors.

4 RESULTS OF THE LTE ANALYSIS

Figs 1–3 show depletion factors versus dust column density for all five regions and Figs 4–6 show depletion factors versus position within each cloud. Average starless and protostellar depletion factors are listed in Table 2. The results will be discussed in detail for each source. We present a more general analysis in Section 5.

4.1 Serpens

The Serpens main cluster, a region of the Serpens molecular cloud particularly rich in star formation, has been extensively studied and shown to contain a population of Class 0/I sources (e.g. see Davis et al. 1999) as well as an apparently older one containing more evolved Class II/III sources (Harvey et al. 2007). Kaas et al. (2004) suggested that the region underwent a burst of star formation roughly 2 Myr ago followed by a later one around 10^5 yr ago. The main cluster is complex, made up of two distinct subclusters, the north-west (NW) and south-east (SE). These two regions are joined by dusty, finger-like structures or filaments. The NW is more quiescent and cooler, whereas the SE is more filamentary, more turbulent

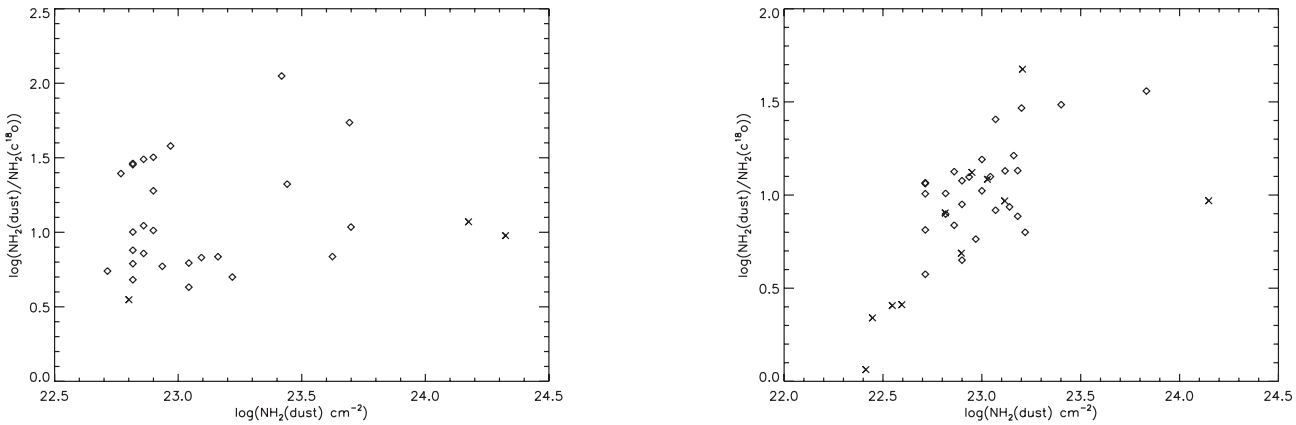

Figure 1. log(H$_2$ column density derived from dust emission) versus log($F_{\rm dep}$) for Orion NGC 2024 (left) and NGC 2071 (right). Squares represent starless cores and crosses protostellar cores.

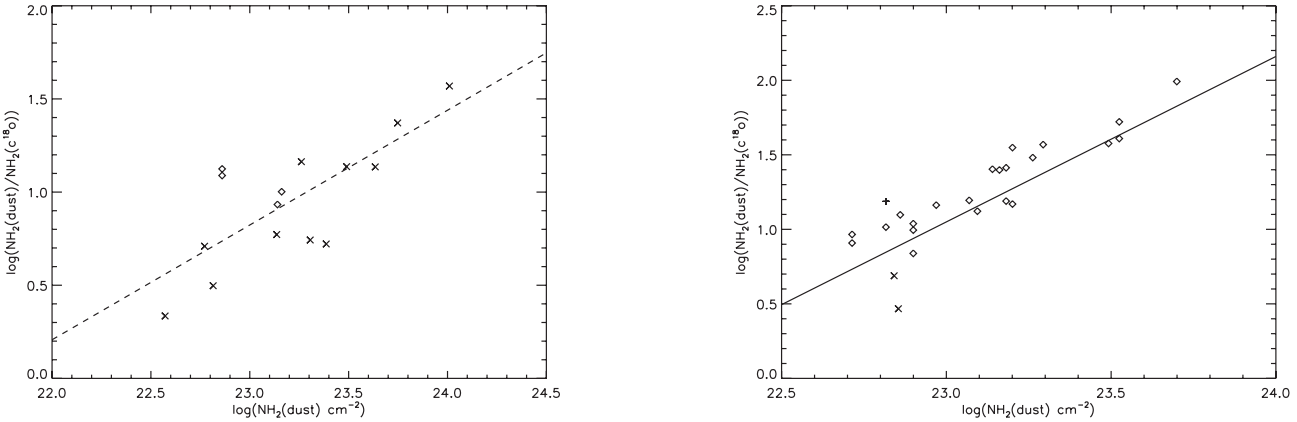

Figure 2. log(H_2 column density derived from dust emission) versus log(F_{dep}) for Serpens (left – dashed line shows the line of best fit of a linear regression on protostellar cores) and Taurus (right – solid line shows the line of best fit of a linear regression on starless cores).

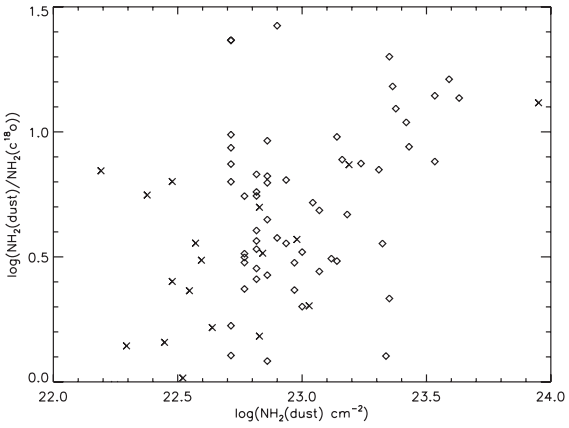

Figure 3. log(H_2 column density derived from dust emission) versus log(F_{dep}) for Ophiuchus.

and hotter (Duarte-Cabral et al. 2010). The Serpens main cluster contains several known Herbig–Haro (HH) objects and outflows (Graves et al. 2010).

Duarte-Cabral et al. (2010) presented a detailed analysis of Serpens using $C^{17}O$ and $C^{18}O$ data from the Institut de Radioastronomie Millimétrique (IRAM) alongside HARP $C^{18}O$ and SCUBA 850-μm maps from the JCMT archive. Their RADEX calculations of CO column density for eight positions spread over the cluster revealed an average discrepancy of roughly a factor of 2.5 between the H_2 densities derived from the dust and those from the CO emission in the NW. This implies some freeze-out of CO. We find higher levels of depletion than these authors in the regions covered by their IRAM data. Bearing in mind that we are looking at only the densest cores in each region, these values are not inconsistent.

We find mean values for F_{dep} of 11 in the starless cores and 12 in the protostellar cores. The largest depletions we find in Serpens are in the centres of protostars located in the NW subcluster (see Fig. 5). In the SE subcluster, depletion factors drop steadily from north to south for both the protostellar and starless cores. If the SE subcluster formed from two colliding filaments (as suggested in Duarte-Cabral et al. 2011, who modelled the cloud using SPH simulations), then perhaps star formation occurred there more rapidly. In this scenario, the NW subcluster could have undergone a slower collapse followed by a burst of star formation. The SE sources cover a larger spread of ages which supports this view. Also, the SE shows higher temperatures, rising towards the interacting region between the two subclusters, probably leading to a release of molecules from dust grains into the gas phase. Note that freeze-out time-scales are short compared to the lifetimes of these clouds. Jones & Williams (1985) estimated a value of $3 \times 10^9/n$ yr, where n is the volume density in cm^{-3}. For densities of up to 10^6 cm^{-3}, such as those seen in pre-stellar cores, this time-scale is much shorter than the lifetime of a typical molecular cloud region ($\sim 10^3$ yr as opposed to $\sim 10^5$ yr for the cloud lifetime). The slower collapse of the NW subcluster

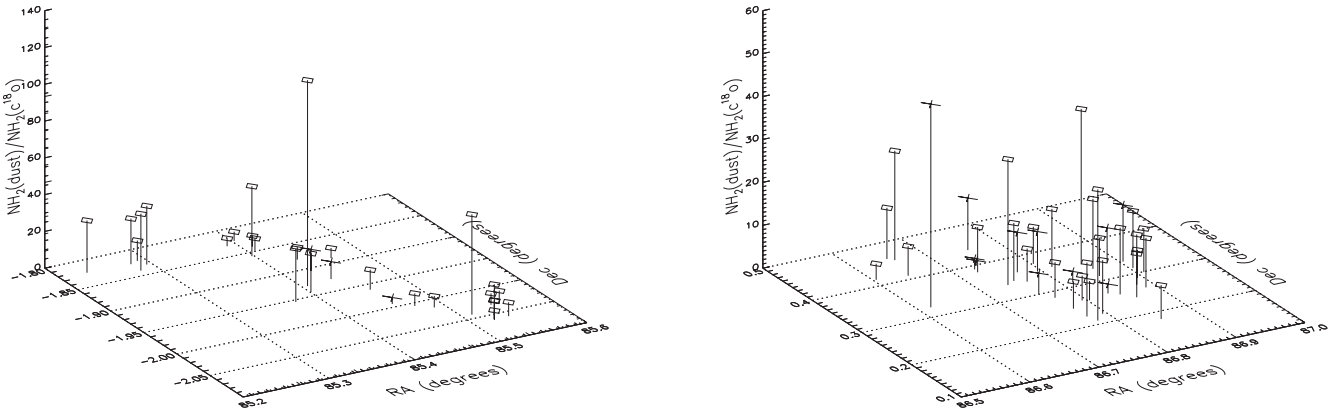

Figure 4. Depletion factor versus position in cloud for Orion NGC 2024 (left) and NGC 2071 (right). Squares represent starless cores and crosses protostellar cores.

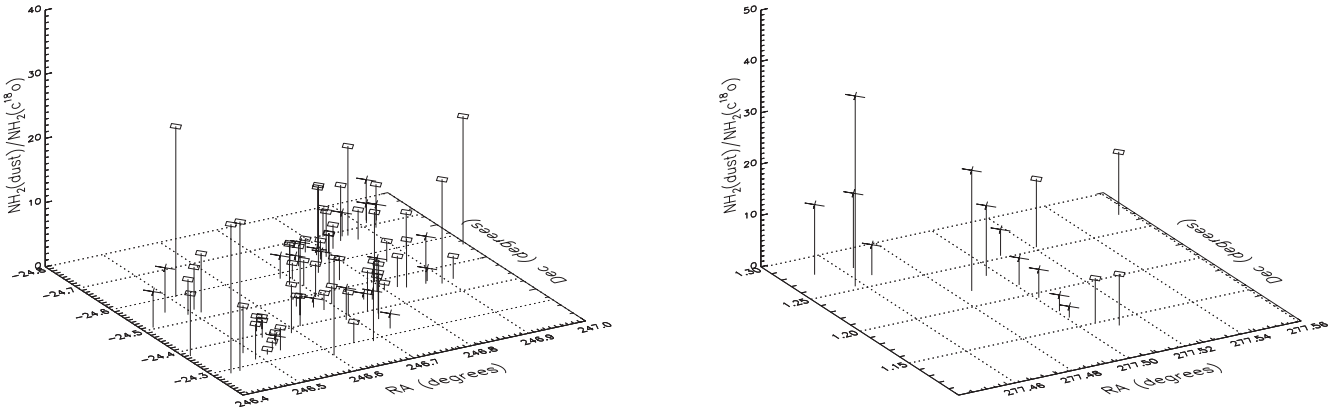

Figure 5. Ophiuchus (left) and Serpens (right).

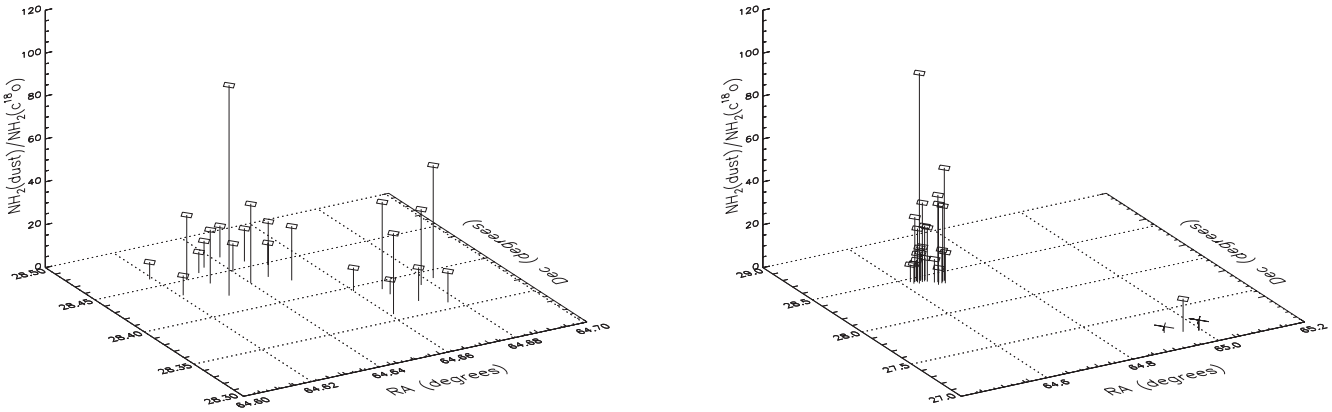

Figure 6. Taurus (left) and Taurus with south-eastern region (right).

Table 2. Depletion factor (F_{dep}) – mean, standard deviation and range. Brackets indicate the number of cores in each sample.

Cloud	Starless mean F_{dep}	Starless F_{dep} sd	Starless F_{dep} range	Protostellar mean F_{dep}	Protostellar F_{dep} sd	Protostellar F_{dep} range	Protostellar mean F_{dep} at 15 K
Serpens	11(4)	2	5	12(11)	10	35	19
Taurus	25(23)	20	91	4(2)	–	–	6
Ophiuchus	7(58)	6	26	4(20)	3	12	6
NGC 2024	19(26)	22	115	8(3)	–	–	13
NGC 2071	13(28)	8	32	10(11)	12	46	16

inferred here would allow more time for freeze-out to occur, hence higher depletion factors in the NW.

Serpens is the only cloud for which protostellar depletion factors are larger on average than those of the starless cores. There are only four starless cores in the sample. Additionally, mean values for this cloud are badly affected by outliers. The median values of F_{dep} for the starless and protostellar cores are 11 and 4, respectively.

4.2 Orion

NGC 2024 and NGC 2071, in contrast to the other clouds discussed here, are both high-mass star-forming regions. As a result, they contain many more O/B-type stars, producing high-velocity outflows and stellar winds that interact with the surrounding cloud material to form complex, filamentary structures. From ^{12}CO and ^{13}CO maps of NGC 2071, White & Phillips (1980) suggested that the region may resemble a rotating disc (at a temperature of around 20 K) with an opaque cloud lying between it and the observer. More recently, Buckle et al. (2010) found NGC 2024 to be the more massive of the two regions and to have a higher average gas temperature (31.8 K as opposed to 19.6 K for NGC 2071). NGC 2071, on the other hand, is dominated by kinetic energy from high-velocity outflows that are at high temperatures compared to the rest of the cloud. Both regions contain optically bright cavities in CO emission surrounded by dust and CO lines. Buckle et al. also commented that the C^{18}O emission in NGC 2071 does not follow the dust emission as closely as it does in NGC 2024, the first possible sign that some CO freeze-out is occurring.

Despite the difference in C^{18}O emission, in general, we find higher levels of depletion in the NGC 2024 cores than in the NGC 2071 cores. We calculate mean values for F_{dep} of 19 in the NGC 2024 starless cores, 8 in the NGC 2024 protostellar cores, 13 in

the NGC 2071 starless cores and 10 in the NGC 2071 protostellar cores. There are a few very depleted cores in the sample so we also consider the median values of $F_{\rm dep}$ which are lower. For NGC 2024 the median value of $F_{\rm dep}$ is 10 for both the starless and protostellar cores. Starless cores in NGC 2071 have a median $F_{\rm dep}$ of 12 in the starless cores and 7 in the protostellar cores. Savva et al. (2003) found depletion factors of around 10 for cores in Orion B. They made use of both $C^{18}O$ and $C^{17}O$ lines, calculating optical depths for each core and using published dust temperatures for each rather than assuming a single temperature for all cores. We do not study exactly the same cores but these values are in rough agreement with average depletions that we calculate for NGC 2024 and NGC 2071. Thomas & Fuller (2008) looked at CO depletion around 84 high-mass sources and found low depletions with a maximum $F_{\rm dep}$ of 10. Again, these values are consistent with our average depletion factors for NGC 2024 and NGC 2071, but our sample contains cores for which we measure much higher depletions, maybe due to an overestimate of the excitation temperature for some cores in these clouds. It is a surprise to find such high depletion factors in high-mass star-forming regions such as NGC 2024 and NGC 2071 because one might expect the hot, turbulent environment to lead to desorption of molecules from grains.

No cores are detected in the NGC 2071 cavity, but rather in the rest of the cloud where the CO emission is stronger. In both NGC 2024 and NGC 2071, the locations of the highly depleted cores all display CO emission but in a more fragmented form (evident in the ^{12}CO maps). This distribution suggests a clumpy medium where parts of the cloud are breaking up to form denser regions conducive to star formation. The dusty regions around the CO cavities are perhaps also active sites of star formation in these clouds. Cores in NGC 2024 show the largest range in calculated depletion factors. The region is hot and turbulent, possibly housing either a more diverse set of objects in terms of their evolution, or cores whose envelopes are affected by surrounding outflows. In both regions, protostellar cores are less depleted on average than starless cores.

4.3 Taurus

The GBS data for Taurus cover a region of the molecular cloud known as L1495. This region contains a compact 'ridge' of CO and dust emission and a 'bowl' of more diffuse emission in the north. The ^{12}CO observations cover the entire ridge and bowl but ^{13}CO and $C^{18}O$ maps are only available for a small section of each, allowing a comparison of conditions in the two regions. The bowl is more evolved than the ridge, containing a larger number of T Tauri stars but fewer molecular outflows (Davis et al. 2010). The ridge is more compact and fragmented.

Ford & Yancy (2011) found very high values of the depletion factor (up to 1000) in Taurus by fitting radiative transfer models to $C^{18}O$ observations, but they admitted finding difficulty in fitting all results well. For a core in L1495, they derived values of around 4 with a fairly large χ^2 value for the best-fitting model. We measure depletion factors around 4–10 times higher for cores in the vicinity, although none of our dust peaks corresponds to exactly the same positions as those investigated by Ford & Yancy. Caselli et al. (1999) found depletion factors of around 10 for the core L1544, also in Taurus.

The only SCUBA protostars identified in the regions observed in the rarer isotopologues of CO are located in the ridge, coincident with two cores identified in HCO^+ by Onishi et al. (2002). In general, levels of depletion are high with mean values for $F_{\rm dep}$ of 25 in the starless cores and 4 in the protostellar cores. The mean is affected by one very highly depleted core, however, and we calculate a slightly lower median value in the starless cores of 15 (again the median value of $F_{\rm dep}$ for the two protostellar cores is 4). A clear divide is found between cores in the bowl and the ridge, though there is a paucity of cores in the latter. In Fig. 6 (right), the bowl comprises the set of starless cores in the top left and the ridge comprises the three cores in the bottom right. Cores in the bowl appear to be much more depleted. This difference could be connected with the lack of outflow activity in the bowl which may be responsible for heating material around cores in the ridge, or may suggest that they are at a more advanced stage of evolution. The two protostars in the ridge are very near HH objects, which is evidence of outflows associated with each. The starless core in the ridge also appears to show low levels of CO depletion, perhaps due to the proximity of the active cores or to its age.

4.4 Ophiuchus

Ophiuchus is the closest of the four clouds in this study, located just 125 pc from the Solar system (Lombardi, Lada & Alves 2008). The GBS images cover the Ophiuchus main cloud core (L1688), a dense region in the centre of the molecular cloud housing many YSOs at varying stages of evolution, including a large population of T Tauri stars. Within the main cloud core, several smaller condensations have been identified in dust continuum maps. These clumps, referred to as Oph A–F, are dense, high extinction regions, probably made up themselves of several sub-clumps that may be star-forming (Friesen et al. 2009; Maruta et al. 2010).

Redman et al. (2002) measured a depletion factor of 10 or so in L1689B in Ophiuchus. That core has a fairly low dust column density (compared to those in our sample) of a few times 10^{22} cm^{-2} so their result agrees well with ours for L1688. Bacmann et al. (2002) measured CO depletion in a sample of nearby pre-stellar cores, some in Ophiuchus and Taurus, by means of $C^{17}O$ and $C^{18}O$ lines. They noted a flattening of the emission profile towards the centres of the cores that they attributed to freeze-out and estimated ratios of 4–15 between observed CO abundances and those inferred from the dust emission.

For Ophiuchus, we find the lowest overall levels of depletion in our sample (a mean $F_{\rm dep}$ of 7 in the starless cores and 4 in the protostellar cores, and a median $F_{\rm dep}$ of 4 in the starless cores and 3 in the protostellar cores). The sample of cores in Ophiuchus was the largest in number but values showed little spread compared to the other clouds. The lowest levels of depletion are in the centre of the imaged region near cores C, E and F with slightly higher values in the starless cores away from the denser, more obscured regions (see Fig. 5). As for the other clouds (with the exception of Serpens), mean protostellar depletions are lower than starless core averages. Studies of the interstellar medium in Ophiuchus suggest that the dust grain size distribution there may be rather unusual, having a population of very large dust grains as well as evidence for very small spinning dust grains (Carrasco, Strom & Strom 1972; Casassus et al. 2008; Chapman et al. 2009). If true, perhaps the reduced surface area available for freeze-out due to the larger grains could partly explain the low levels of depletion seen here. Past studies (e.g. Friesen et al. 2009) also suggest that the gas temperature in Ophiuchus may be high compared to other, similar regions. From our CO measurements, we calculate temperatures for the starless and protostellar cores that are intermediate between those in Orion and the lower temperatures of Taurus and Serpens. However, if temperatures were higher the low levels of depletion could be explained by desorption.

5 GLOBAL ANALYSIS OF DEPLETION DATA

5.1 Comparison of sources and previous results

We see a large range in $F_{\rm dep}$ from unity (no depletion) up to 112 in NGC 2024. Table 2 lists average values of $F_{\rm dep}$ for both the protostellar and starless cores in all five regions. Overall, levels of CO depletion are highest in Taurus and NGC 2024 and lowest in Ophiuchus. The fact that we see the largest levels of depletion in Taurus and NGC 2024, the two most contrasting clouds in terms of their physical conditions (one being cool and fairly quiescent and the other hot and turbulent), is interesting. Core samples for both clouds are made up mainly of starless cores and for both there is a large spread in derived depletion factors. In Orion, the depletion factors in cores track much less well the core dust column densities. The majority of the cores are not very depleted, with a couple of very highly depleted cores affecting the mean.

The highest values of $F_{\rm dep}$ that we find are large compared to most past studies of which we are aware. We cover, however, many more sources in our study and the average depletion factors we find are in fair agreement with previously derived values. Table 3 compares values from the literature with ours for the same clouds. Even taking into account errors, which in most cases will cause us to overestimate the depletion factor (see Section 6), this possibility cannot completely explain the extremely high depletions found in some cores. The JCMT beam for both the line and continuum data at the wavelengths we use is small so we are looking at the very centres of the cores, where one would expect to see higher depletion factors, rather than an average over a larger region. There are only a few very highly depleted cores (around 6 with an $F_{\rm dep}$ higher than 40). All but one of these are classified as starless and are probably older, more evolved cores for which molecules have had more time to deplete.

5.2 Density versus depletion correlation

There is some evidence of correlation between the column densities of the cores and the depletion factor in the case of starless cores in Taurus and protostellar cores in Serpens. A linear regression analysis yields high values of the coefficient of determination (R^2), an indicator of how well a particular linear model fits the data (e.g. an R^2 value of 0.8 indicates that 80 per cent of the variance in the data can be explained by a particular model, and the model is usually considered a good fit). Cores in Serpens and starless cores in Taurus have linear fits with R^2 values above 0.8. The best-fitting lines for these clouds are plotted in Fig. 2. The correlations are different for the two clouds (see Table 4 for values of the intercept and slope in each case), the relation for Serpens being shallower. This distinction could indicate differences in the behaviour of starless and protostellar cores. Our sample of cores in Serpens is a more evolved population for which some heating of the core centre causes a release of molecules into the gas phase. Results for Orion and Ophiuchus do not point to any correlation between depletion and core column density or mass, however.

In Fig. 7, depletion factors are plotted against dust column density for all cores in all clouds in the sample. In the right-hand plot, the slopes of the two significant correlations have been added, representing the increase in depletion with core density for Serpens and Taurus. The data are suggestive of perhaps containing two populations, one similar to the starless cores in Taurus and one similar to the protostars in Serpens, whose depletions vary differently with core column density. The protostellar cores do tend to exhibit a shallower slope. There are many fairly undepleted starless cores at high densities, but it could be that some of these cores house undetected protostars. This relation would have to be confirmed using SCUBA-2 or Atacama Large Millimeter Array (ALMA) observations of these regions for a much larger sample of cores.

Table 4. Density–depletion correlation.

Cloud	Intercept[a]	Gradient[a]	Coefficient of determination (R^2)	$N_{\rm cores}$
Serpens	3.98	3.10(−23)	0.81	15
Serpens protostellar	1.49	3.48(−23)	0.91	11
Taurus	−3.67	1.73(−22)	0.89	25
Taurus starless	−2.33	1.70(−22)	0.88	23
Ophiuchus	4.13	1.64(−23)	0.14	78
Ophiuchus starless	4.34	2.01(−23)	0.10	58
Ophiuchus protostellar	2.59	1.20(−23)	0.58	20
NGC 2024	18.43	−6.16(−25)	0.00	29
NGC 2024 starless	12.56	4.76(−23)	0.08	26
NGC 2071	10.68	9.93(−24)	0.06	39
NGC 2071 starless	6.83	4.86(−23)	0.51	28
NGC 2071 protostellar	9.83	2.10(−24)	0.00	11

[a]Units for the intercept and gradient are the same as for Figs 1–3. (The intercept is unitless and the gradient has units of cm^3.)

5.3 Protostellar versus starless core depletion

On average, CO appears to be more depleted in starless cores than protostellar cores (other than in Serpens for which the sample contains only four starless cores and mean values are affected by outliers). Levels of depletion should relate to both the time-scale of envelope accretion and the stage of evolution of the central radiation source for protostellar cores since both affect the freeze-out time-scale. Overall, protostellar cores with high densities tend not

Table 3. A comparison with previous studies.

Paper reference	Region	$F_{\rm dep}$	Our mean starless $F_{\rm dep}$	Our mean protostellar $F_{\rm dep}$
Caselli et al. (1999)	Taurus	10	25	4
Bacmann et al. (2002)		14		
Ford & Yancy (2011)		4–1000		
Bacmann et al. (2002)	Ophiuchus	4.5–14	7	4
Redman et al. (2002)		10		
Savva et al. (2003)	Orion B	10	19/13[a]	8/10[a]
Duarte-Cabral et al. (2010)	Serpens	2.5	11	12

[a]Values quoted for NGC 2024 (left) and NGC 2071 (right).

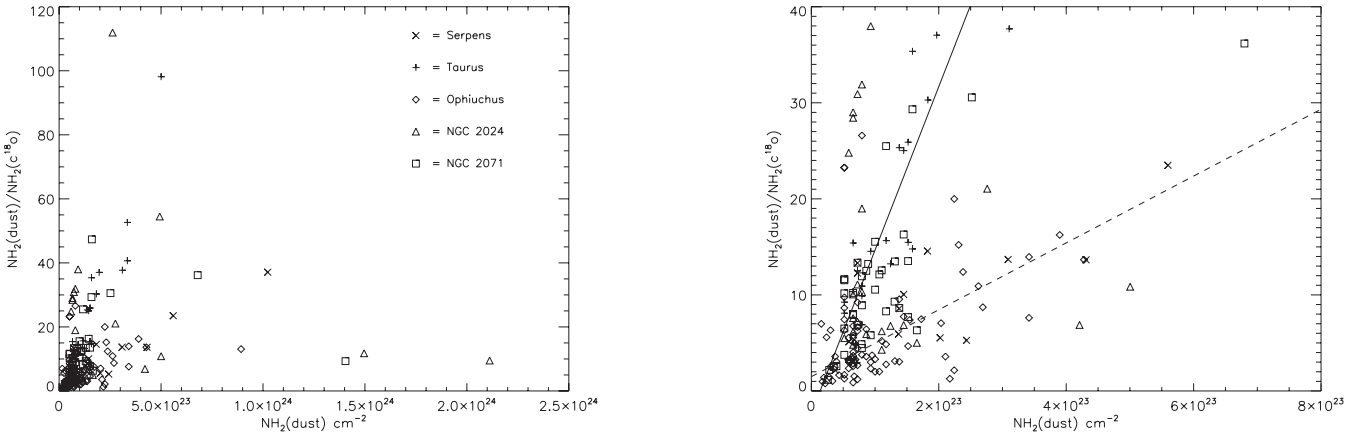

Figure 7. $F_{\rm dep}$ versus dust column density for all clouds. Trends are plotted for Serpens (dotted line) and Taurus (solid line).

to be very depleted in comparison with dense starless cores in the same cloud. Jørgenson, Schöier & van Dishoeck (2005) looked at depletion profiles across 16 protostellar cores and found that the size of the depletion zone grew with envelope mass in the early stages of evolution and then shrink as the central star began to heat the inner regions. Perhaps we see here that higher mass protostars are in a more advanced stage of evolution where a substantial envelope has been formed (hence the higher dust column densities) and the central star has begun to evaporate material from the grains in the centre. It would be useful to model in more detail a selection of cores from each cloud to get a handle on ages, density structures and a more accurate measure of depletion. It should be noted that, in crowded environments, the infrared observations towards several cores may be misinterpreted or contaminated by the infrared emission from nearby, more evolved YSOs or from a brighter, diffuse infrared background. Therefore, very faint protostellar emission, such as from Very Low Luminosity Objects (VeLLOs; Pineda et al. 2011), in these regions may be misclassified.

6 UNCERTAINTIES IN THE LTE DERIVED DEPLETION FACTOR

The calculation of column densities via LTE does of course have drawbacks. The temperatures used to derive hydrogen column densities from CO are uncertain since they are roughly calculated, more than one rotational transition of a given molecule not being available. The CO temperatures are derived from the ^{12}CO and ^{13}CO profiles which may well arise in hotter regions of the cloud, being self-absorbed in the core centre. In such a case, the use of these lines would result in an artificially high C^{18}O temperature and low abundance being derived, leading to overestimates of the CO depletion. Furthermore, the exponential factor including $T_{\rm ex}$ in equation (2) for calculating CO column density rises rapidly below about 20 K, so the difference between assuming a temperature of 20 and 10 K leads to a factor of around 2.5 difference in the derived depletion factor.

As a test, calculations were performed as above, this time fixing the C^{18}O excitation temperatures to the assumed dust temperatures (10 K for starless cores and 20 K for the protostars). Since temperatures derived from ^{12}CO and ^{13}CO are near 10–15 K in general, little difference to what is shown in Figs 1–3 was seen. The only major discrepancy was in the case of NGC 2024, for which several very high excitation temperatures are derived from the two more common isotopologues of CO. Here, protostellar depletion factors remain similar but the starless cores show far lower levels of depletion in most cases. Figs 8 and 9 show depletion plots for NGC 2024 and Serpens using temperatures derived from the CO isotopologues themselves (left) and setting C^{18}O temperatures equal to dust temperatures (right – note the different scales on the *y*-axis for NGC 2024). Depletion factors may be particularly influenced

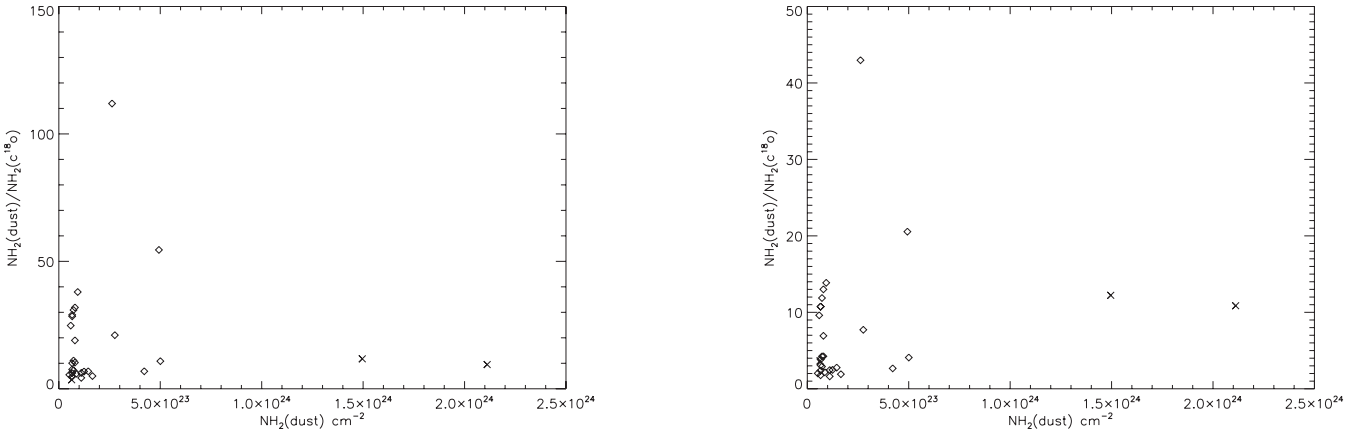

Figure 8. Orion NGC 2024 using CO-derived temperatures to estimate $F_{\rm dep}$ (left) and using dust temperatures (right). Squares represent starless cores and crosses protostellar cores.

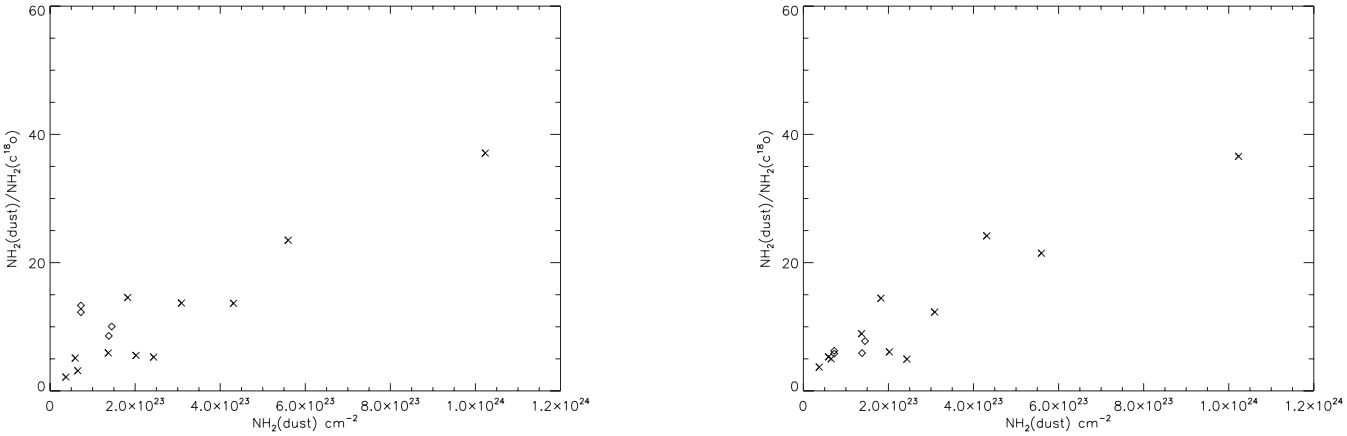

Figure 9. Serpens using CO-derived temperatures to estimate $F_{\rm dep}$ (left) and using dust temperatures (right).

by the temperature estimation in this cloud since the isotopologues used to calculate temperatures will trace the hotter surrounding regions (due to higher optical depth in the denser regions) which may be more diverse physically, or contrast more with the dense core centres, than for the other regions due to the filamentary structure and outflow activity.

A major cause of error in our results may be the assumption of optically thin $C^{18}O$ in the core centres. Higher optical depth in that line could lead to an underestimate of the CO gas phase abundance and hence an overestimate of the depletion. We estimated $C^{18}O$ opacities very roughly using fig. 12 from Curtis, Richer & Buckle (2010) showing the variation of the $C^{18}O$ opacity with the ratio of the ^{13}CO to $C^{18}O$ line peaks for $X(^{13}CO)/X(C^{18}O)$ equal to 7.3 (Wilson & Rood 1994). Using the ratios of the peak ^{13}CO and $C^{18}O$ temperatures at the dust peaks, we estimated $C^{18}O$ opacities for the cores. Values were primarily very low and greater than 1 in only 25 of the 370 cores in our sample. Correcting equation (2) using our derived value of the optical depth made very little difference to the resultant plots. Note, however, that the same method is used for all cores in all clouds, so that while derived individual values of $F_{\rm dep}$ may suffer from these uncertainties a comparison between regions should still be possible.

The beam size of the JCMT (14 arcsec for the CO maps) is generally smaller than CLUMPFIND-derived diameters for the dust cores, so we do not consider beam dilution effects to be a problem and assume a beam filling factor of 1 in all cases.

The calculation of molecular hydrogen column density from $C^{18}O$ emission requires the assumption of a constant $N(C^{18}O)/N(H_2)$ ratio. Published values vary by a factor of $\sim$7 from 0.7×10^{-7} (Tafalla & Santiago 2004) to 4.8×10^{-7} (Lee et al. 2003). We adopt the value quoted in Frerking et al. (1982) and note that this choice may influence our calculated depletion factors differently in different regions.

In our dust column density calculations, we assume fixed dust temperatures of 10 K for the starless cores and 20 K for the protostars. Using the higher temperature for the protostellar cores results in lower densities being derived from the dust and so lower values of the depletion factor for these cores. For the protostellar cores, there will likely be some local heating of the dust near to the core centres, so we adopt 20 K. Modelling work in the past has suggested that dust temperatures for Class 0 and Class I sources may be closer to 15 K than the 20 K assumed here (Shirley, Evans & Rawlings 2002; Young et al. 2003), though with fairly significant spreads in derived temperatures (4.8 K for the former and 8 K for the latter). In addition, Larsson et al. (2000) studied the spectral energy distributions of five submillimetre sources in Serpens and derived dust temperatures of around 30 K for those sources. Given these differences, it is somewhat unrealistic to define a single dust temperature for the cores. As a test, we re-calculated depletion factors assuming a dust temperature for all the cores of 15 K. In this instance, protostellar core depletion factors rise by a factor of only 1.6 compared to those calculated assuming 20 K, so this is probably not a major effect compared to other assumptions we make.

Depletion factors may be underestimated due to the larger beam size of the telescope at 850 μm relative to that of the spectral line data (22.9 and 14 arcsec, respectively). The SCUBA beam will sample a larger area around the dust cores so that the flux will be slightly diluted compared to the CO maps which sample the more central regions of the cores. Although both beams are smaller than the core diameters (from CLUMPFIND), our assumption of an even distribution of material across the cores will not be accurate.

The 850-μm fluxes and the $C^{18}O$ peak line temperatures also have associated uncertainties due to the underlying noise in the data (30 mJy for the SCUBA data, see Table 1 for the CO rms noise values). We estimate the error on the calculated depletion factor for a typical starless core in Serpens and derive an error of ± 1.47 on a depletion factor of 10. This is likely to be similar for other cores (less for those with brighter emission) and is not significant compared to some of the uncertainties mentioned above.

The ^{12}CO $J = (3 \rightarrow 2)$ line falls within the SCUBA 850-μm band so we investigated the possible effect of contamination of the dust emission. Recent work suggests that the highest levels of contamination occur in molecular outflow regions rather than in quiescent cores. In these cases, the CO flux contribution can reach around 0.40 Jy beam^{-1} (in grade 2 weather for one of the outflows of NGC 2071) and is estimated to be much lower for the regions studied here, at most 25 per cent of the total peak flux and usually much less. This would result in a reduction in $N_{\rm H_2\,dust}$ of 25 per cent with an equivalent decrease in the resulting depletion factor. This is, however, a worst-case scenario and errors resulting from contamination will probably be far lower in most cases (Emily Drabek, private communication).

7 EVALUATING DEPLETION FACTORS USING RADEX

We used RADEX (van der Tak et al. 2007), a radiative transfer code approximating a large velocity gradient (LVG) approach, to calculate

CO column densities and derive alternative depletion factors. RADEX and LTE are both approximations. In LTE, the Boltzmann equation accurately describes the level populations for any molecule, with the excitation temperature of all lines equal to the gas kinetic temperature. RADEX, on the other hand, takes into account both collisions and the local radiation field. It does not, however, include any external radiation field. Using both methods should allow us to probe the range of conditions in the clouds. White, Casali & Eiroa (1995) compared $C^{18}O$ column densities in the Serpens molecular cloud calculated using LTE and LVG methods. They found that, particularly for cooler, dense material, LTE methods tended to underestimate column densities compared to LVG calculations by factors of around 4–8 at 10 K.

To solve the level populations, RADEX uses the escape probability method to describe the effect of the radiation field. RADEX allows for the use of several different geometries which affect the escape probability calculations. Here we used a homogeneous sphere having tested other geometries and found the choice made little difference to the results. For the RADEX calculations, two grids of models were run, one for the ^{13}CO data and one for the $C^{18}O$ data. For both, the column density of the molecule and the gas kinetic temperature were left as free parameters. The dust density was fixed using the 850-μm emission exactly as for the LTE calculations and converted to a volume density using the CLUMPFIND derived core sizes. We measured line widths from the HARP ^{13}CO and $C^{18}O$ spectra at the peak of the dust emission. We then assumed a canonical ratio of 7.3

Table 5. LTE and RADEX results – Taurse refers to the south-eastern region of L1495 (the ridge). Brackets indicate powers of 10.

Core	RA (J2000)	Dec. (J2000)	Rad (pc)	Density of gas[a] (cm^{-3})	Column density of gas (cm^{-3})	T_{ex} (LTE)	F_{dep} (LTE)	T_{kin} (RADEX)	F_{dep} (RADEX)	Reduced χ^2
Oph p3	$16^h26^m10^s4$	$-24°20''56'$	0.027	4.0(5)	6.74(22)	35 K	2	37 K	1	8.69
Oph p4 ↑*	$16^h26^m27^s6$	$-24°23''57'$	0.054	2.7(6)	8.93(23)	29 K	13	28 K	0	267.88
Oph p10	$16^h27^m00^s5$	$-24°26''38'$	0.017	1.7(5)	1.76(22)	23 K	1	28 K	1	2.07
Oph p13	$16^h27^m07^s2$	$-24°38''08'$	0.023	2.3(5)	3.32(22)	18 K	1	14 K	1	2.09
Oph s18	$16^h26^m36^s3$	$-24°17''56'$	0.026	6.2(5)	1.00(23)	27 K	3	22 K	2	5.51
Oph s42	$16^h27^m58^s6$	$-24°33''43'$	0.033	1.0(6)	2.24(23)	17 K	20	12 K	14	0.09
Oph s53	$16^h27^m05^s0$	$-24°39''14'$	0.029	1.3(6)	2.24(23)	18 K	2	10 K	3	0.43
Taurse p1	$04^h19^m42^s3$	$27°13''37'$	0.024	4.8(5)	7.15(22)	12 K	3	8 K	2	0.07
Taurse p2	$04^h19^m58^s4$	$27°10''00'$	0.026	4.3(5)	6.95(22)	12 K	5	12 K	4	0.17
Taurse s1	$04^h19^m50^s8$	$27°11''30'$	0.019	5.6(5)	6.56(22)	9 K	8	10 K	16	0.04
Taur s9	$04^h18^m33^s6$	$28°26''53'$	0.008	2.5(6)	1.24(23)	10 K	13	10 K	7	0.25
Taur s18 *	$04^h18^m38^s7$	$28°21''30'$	0.009	5.6(6)	3.11(23)	11 K	38	8 K	4	0.02
Taur s21 *	$04^h18^m41^s0$	$28°22''00'$	0.006	9.1(6)	3.35(23)	11 K	16	8 K	9	0.80
Taur s22 *	$04^h18^m42^s4$	$28°21''30'$	0.006	1.8(6)	6.56(22)	11 K	15	8 K	2	0.21
Taur s24 ↑*	$04^h18^m43^s7$	$28°23''24'$	0.012	4.5(6)	3.35(23)	11 K	53	7 K	1	1.38
Serp p2	$18^h29^m49^s8$	$01°16''39'$	0.055	3.0(6)	1.02(24)	21 K	37	13 K	14	0.06
Serp p3	$18^h29^m51^s4$	$01°16''33'$	0.038	7.8(5)	1.82(23)	20 K	15	14 K	9	0.46
Serp p8	$18^h30^m00^s2$	$01°10''21'$	0.037	2.9(5)	6.53(22)	13 K	3	10 K	1	0.45
Serp p9	$18^h30^m00^s2$	$01°11''39'$	0.053	6.2(5)	2.02(23)	17 K	6	14 K	5	1.42
Serp p11	$18^h30^m01^s8$	$01°15''09'$	0.035	2.7(5)	5.91(22)	19 K	5	26 K	6	0.19
Serp s2	$18^h30^m02^s6$	$01°09''03'$	0.028	8.4(5)	1.45(23)	11 K	10	11 K	5	0.87
Serp s3	$18^h30^m05^s0$	$01°15''15'$	0.022	5.4(5)	7.25(22)	18 K	13	64 K	10	11.38
Serp s4	$18^h30^m13^s4$	$01°16''15'$	0.032	3.7(5)	7.25(22)	15 K	12	31 K	15	0.03
NGC 2024 p1 *td*	$05^h41^m43^s0$	$-01°54''20'$	0.168	6.9(4)	7.15(22)	59 K	12	64 K	0	28.44
NGC 2024 p2 *td*	$05^h41^m44^s6$	$-01°55''38'$	0.233	5.7(4)	8.18(22)	71 K	10	80 K	0	147.78
NGC 2024 p3 *t*	$05^h41^m49^s4$	$-01°59''38'$	0.084	4.0(4)	2.05(22)	22 K	4	24 K	1	14.21
NGC 2024 s29	$05^h41^m33^s4$	$-01°49''50'$	0.044	4.0(5)	1.10(23)	24 K	4	80 K	3	17.57
NGC 2024 s31 *t*	$05^h41^m36^s2$	$-01°56''32'$	0.120	3.7(5)	2.76(23)	36 K	21	80 K	7	697.60
NGC 2024 s39	$05^h42^m03^s1$	$-02°04''21'$	0.064	2.0(5)	7.94(22)	20 K	10	35 K	11	0.19
NGC 2024 s40	$05^h42^m05^s9$	$-02°03''33'$	0.067	1.6(5)	6.56(22)	16 K	10	72 K	7	32.57
NGC 2024 s47	$05^h41^m36^s6$	$-01°49''26'$	0.056	4.8(5)	1.66(23)	43 K	5	80 K	3	69.31
NGC 2024 s53	$05^h42^m02^s7$	$-02°02''33'$	0.104	7.7(5)	4.93(23)	25 K	54	24 K	46	0.55
NGC 2071 p3	$05^h46^m55^s0$	$00°23''26'$	0.055	1.0(5)	3.52(22)	21 K	3	14 K	1	1.15
NGC 2071 p10 *t*	$05^h47^m20^s2$	$00°16''02'$	0.053	9.6(4)	2.80(22)	25 K	2	28 K	2	5.23
NGC 2071 p12	$05^h47^m37^s0$	$00°20''02'$	0.087	1.7(5)	8.91(22)	15 K	13	17 K	13	0.24
NGC 2071 s3	$05^h46^m36^s2$	$00°27''32'$	0.052	2.5(5)	7.94(22)	16 K	12	13 K	7	0.30
NGC 2071 s17 *t*	$05^h47^m12^s6$	$00°15''38'$	0.048	2.7(5)	7.94(22)	28 K	4	33 K	4	16.14
NGC 2071 s23	$05^h47^m31^s4$	$00°16''26'$	0.040	2.1(5)	5.18(22)	20 K	12	35 K	13	0.04

[a]Values inferred from observations of the dust emission using the method outlined in Section 3.
*Many equally good fits were achieved so there was no unique model fit to the data.
↑The $C^{18}O$ peak for the line is higher than the ^{13}CO peak.
*t*The ^{13}CO line peak is higher than the ^{12}CO peak (and hence is more likely to be optically thick or self-absorbed).
*td*The ^{13}CO profile is double peaked.

between the ^{13}CO and the C^{18}O abundances (Wilson & Rood 1994). The best-fitting output to the observed line intensities of both ^{13}CO and C^{18}O was selected by minimizing the value of the reduced χ^2 parameter given by

$$\frac{(I_{18\mathrm{obs}} - I_{18\mathrm{mod}})^2}{(\Delta I_{18\mathrm{obs}})^2} + \frac{(I_{13\mathrm{obs}} - I_{13\mathrm{mod}})^2}{(\Delta I_{13\mathrm{obs}})^2}, \quad (5)$$

where I_{obs} and I_{mod} are the observed and modelled peak line intensities. This method assumes that ^{13}CO and C^{18}O are tracing the same gas though this may not be the case.

7.1 LTE versus RADEX

Both the RADEX and LTE results are shown in Table 5 as well as some properties of the cores from the Sadavoy et al. (2010) catalogue. We did not analyse all cores with RADEX but chose a few to get some idea of how different the results from RADEX and LTE would be and how effectively RADEX could be used with the data available to evaluate depletion factors. We selected cores from a variety of positions within the cloud, and with varying properties.

Table 5 lists an identifier for each core, its position, the (CLUMPFIND defined) radius, dust density, dust column density, temperature derived from the ^{12}CO lines in LTE, depletion derived in LTE, gas kinetic temperature from RADEX and the depletion factor calculated with RADEX. The final column lists the reduced χ^2 value, intended to give an idea of how well the best-fitting model and observed values agree in each case. We consider values of this parameter below 2 to indicate a good fit (with the gas kinetic temperature and the ^{13}CO and C^{18}O column densities as free parameters). Note again that a depletion factor of 1 indicates no depletion.

In Table 5, there are three cores for which values of F_{dep} are equal to 0 as calculated by RADEX indicating that the column density of hydrogen calculated using the dust emission was a lot lower than that calculated using the gas phase CO emission. In these cases, the RADEX kinetic temperature was higher than 25 K. If correct, it is likely that the CO in these cases emanates from warmer regions outside of the dense cores. The χ^2 values for these cores were also all high.

In most cases, RADEX and the LTE approximation yielded similar values for the depletion factor and gas kinetic temperature. There appears, however, to be a tendency towards lower depletion estimates when using RADEX rather than LTE. Several cores, particularly those in Taurus and NGC 2024, were very difficult to fit using RADEX (either never finding a good fit, indicated by the high values for the fit parameter in Table 5, or else finding equally good fits for several input combinations, marked by an asterisk in the table). Other than six cores, four of which are in NGC 2024, kinetic temperatures derived via the two methods agree to within 4–5 K on average. We note that the maximum depletion factor we calculate for the cores in Serpens is similar to that found by Duarte-Cabral et al. (2010).

Fig. 10 shows LTE versus RADEX derived depletion factors. The left-hand plot includes the full sample of fitted cores (with starless cores as squares and protostellar cores as crosses). The right-hand plot shows only those for which we could find a fairly good unique fit with RADEX (χ^2 less than 2). Looking at the right-hand plot, it does appear that for several cores (two in particular) LTE methods overestimate CO depletion (or underestimate column densities). The two cores for which this effect is most prominent are the two densest cores in the sample. If LTE line intensities reach a maximum for a given column density, and if the population is sub-thermal, a higher column density of CO is required to reach the same line intensities. Where LTE depletions are high may be a result of high optical depth in the C^{18}O line, resulting in an underestimate of CO gas column density in the LTE approximation. On the other hand, using the ^{13}CO line in the RADEX models may lead to problems due to self-absorption in that line.

Cores with very different depletion factors derived from the two methods did tend to display double-peaked ^{13}CO line profiles or have higher intensities in the C^{18}O line than the ^{13}CO, both indications of self-absorption. We also use core sizes from the code CLUMPFIND to calculate dust volume densities to input into RADEX, which may introduce further uncertainty. The fact that we have only one transition for each isotopologue of CO is likely the main cause of error when using RADEX to estimate column densities. It is encouraging that temperatures, depletions and general trends agree to some extent in those cores for which we could achieve a good fit (a median discrepancy of 2 in the depletion factor and 4 K in the temperature). To use this code to find depletion factors for all cores and properly compare regions, we would need a good and unique fit for all cores. It would be preferable to obtain data with several transitions for C^{18}O rather than using two isotopologues.

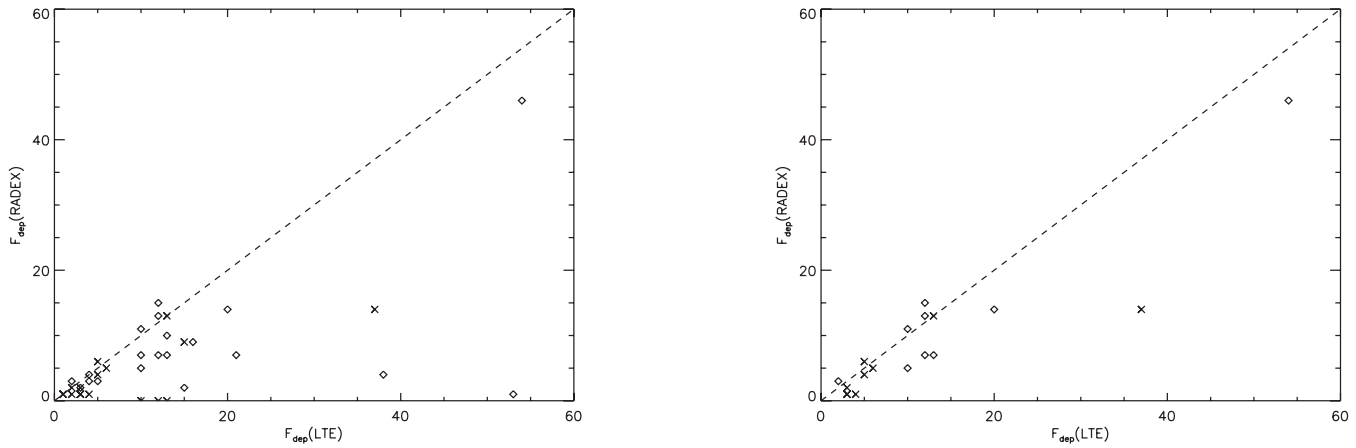

Figure 10. RADEX versus LTE depletion factors. Left: all cores fitted with RADEX (starless cores are squares, protostellar cores are crosses). Right: only cores with a good (χ^2 less than 2), unique RADEX fit.

8 SUMMARY

We have used the $C^{18}O$ and dust emission in dense cores within five local star-forming regions, experimenting with both LTE and non-LTE methods, to compare statistically large-scale depletion factors. We find the following.

(i) Within each cloud, the highest levels of depletion are found in the longer lived regions (Serpens and Taurus) or fragmented regions around the edges of CO cavities (Orion).

(ii) Cores in Ophiuchus (L1688) are the least depleted overall. This behaviour could be connected to the anomalous grain size distribution inferred from observations of this cloud.

(iii) There is a strong correlation between core density and depletion in both Serpens and Taurus.

(iv) Starless cores are, on average, more depleted than protostellar cores (an overall mean depletion factor of 13 rather than 7) and protostars may show a different trend with core density to the starless cores. This could be due to the evaporation of material from dust grains after heating by nearby sources.

We note that while our study suffers from uncertainties due to temperature estimations and the assumption of LTE, these are often systematic and should not affect comparison of depletion factors among the different clouds. These factors do, however, affect the depletion factors derived for individual cores. Multiline observations of $C^{18}O$ as well as other isotopologues should help to constrain better the CO column densities and temperatures and achieve more accurate measures of the depletion factors.

ACKNOWLEDGMENTS

We would like to thank the referee for very helpful comments and careful reading, and the Gould Belt Survey team.

REFERENCES

Aikawa Y., Ohashi N., Inutsuka S., Herbst E., Takakuwa S., 2001, ApJ, 552, 639
Bacmann A., Lefloch B., Ceccarelli C., Castets A., Steinacker J., Loinard L., 2002, ApJ, 389, 6
Buckle J. V. et al., 2009, MNRAS, 399, 1026
Buckle J. V. et al., 2010, MNRAS, 401, 204
Buckle J. V. et al., 2011, MNRAS, in press (doi:10.1111/j.1365-2966.2012.20628.x)
Carrasco L., Strom S. E., Strom K. M., 1972, ApJ, 182, 95
Casassus S. et al., 2008, MNRAS, 391, 1075
Caselli P., Walmsley C. M., Tafalla M., Dore L., Myers P. C., 1999, ApJ, 523, 165
Chapman N. L., Mundy L. G., Lai S.-P., Evans N., 2009, ApJ, 690, 496
Curtis E. I., Richer J. S., Buckle J. V., 2010, MNRAS, 401, 455
Davis C. F., Matthews H. E., Ray T. P., Dent W. R. F., Richer J. S., 1999, MNRAS, 309, 141
Davis C. J. et al., 2010, MNRAS, 405, 759
Di Francesco J., Evans N. J., II, Caselli P., Myers P. C., Shirley Y., Aikawa Y., Tafalla M., 2007, in Reipurth B., Jewitt D., Keil K., eds, Protostars and Planets V. Univ. Arizona Press, Tucson, p. 17
Di Francesco J., Johnstone D., Kirk H. M., MacKenzie T., Ledwosinska E., 2008, ApJS, 175, 277
Duarte-Cabral A., Fuller G. A., Peretto N., Hatchell J., Ladd E. F., Buckle J., Richer J., Graves S. F., 2010, A&A, 519, 27
Duarte-Cabral A., Dobbs C. L., Peretto N., Fuller G. A., 2011, A&A, 528, 50
Frerking M. A., Langer W. D., Wilson R. W., 1982, ApJ, 262, 590
Friesen R. K., Di Francesco J., Shirley Y. L., Myers P. C., 2009, ApJ, 697, 1457
Graves S. F. et al., 2010, MNRAS, 409, 141
Harvey P. M., Merín B., Huard T. L., Rebull L. M., Chapman N., Evans N. J., II, Myers P. C., 2007, ApJ, 663, 1149
Jones A. P., Williams D. A., 1985, MNRAS, 217, 413
Jørgenson J. K., Schöier F. L., van Dishoeck E. F., 2005, A&A, 435, 177
Kaas A. A. et al., 2004, A&A, 421, 623
Larsson B. et al., 2000, A&A, 363, 253
Lombardi M., Lada C. J., Alves J., 2008, A&A, 480, 785
Maruta H., Nakamura F., Nishi R., Ikeda N., Kitamura Y., 2010, ApJ, 714, 680
Muñoz Caro G. M., Jiménez-Escobar A., Martín-Gago J. Á., Rogero C., Atienza C., Puertas S., Sobrado J. M., Torres-Redondo J., 2010, A&A, 522, 108
Nakagawa N., 1980, in Andrew B. H., ed., Proc. IAU Symp. 87, Interstellar Molecules. Reidel, Dordrecht, p. 365
Öberg K. I., Garrod R. T., van Dishoeck E. F., Linnartz H., 2009, A&A, 504, 891
Öberg K. I., Boogert A. C. A., Pontoppidean K. M., van den Broek S., van Dishoeck E. F., Bottinelli S., Blake G. A., Evans N. J., II, 2011, ApJ, 740, 1090
Onishi T., Mizuno A., Kawamura A., Tachihara K., Fukui Y., 2002, ApJ, 575, 950
Ossenkopf V., Henning T., 1994, A&A, 291, 943
Pineda J. E., Caselli P., Goodman A. A., 2008, ApJ, 679, 481
Pineda J. E. et al., 2011, ApJ, 743, 201
Rawlings J. M. C., Hartquist T. W., Menten K. M., Williams D. A., 1992, MNRAS, 255, 471
Redman M. P., Rawlings J. M. C., Nutter D. J., Ward-Thompson D., Williams D. A., 2002, MNRAS, 337, 17
Roberts J. F., Rawlings J., Viti S., Williams D. A., 2007, MNRAS, 382, 733
Sadavoy S. I. et al., 2010, ApJ, 710, 1247
Savva D., Little L. T., Phillips R. R., Gibb A. G., 2003, MNRAS, 343, 259
Shirley Y. L., Evans N. J., Rawlings J. M. C., 2002, ApJ, 575, 337
Taylor S. D., Williams D. A., 1996, MNRAS, 282, 1343
Thomas H. S., Fuller G. A., 2008, A&A, 479, 751
van der Tak F. F. S., Black J. H., Schöier F. L., Jansen D. J., van Dishoeck E. F., 2007, A&A, 468, 627
van Dishoeck E. F., 2004, ARA&A, 42, 119
Viti S., Girart J. M., Garrod R., Williams D. A., Estalella R., 2003, A&A, 399, 187
Ward-Thompson D. et al., 2007, PASP, 119, 855
Warren-Smith R. F., Wallace P. T., 1993, in Hanisch R. J., Brissenden R. J. V., Barnes J., eds, ASP Conf. Ser. Vol. 52, Astronomical Data Analysis Software and Systems II. Astron. Soc. Pac., San Francisco, p. 229
White G. J., Phillips J. P., 1980, MNRAS, 194, 947
White G. J., Casali M. M., Eiroa C., 1995, A&A, 298, 594
Williams J. P., de Geus E. J., Blitz L., 1994, ApJ, 428, 693
Wilson T. L., Rood R., 1994, A&A, 32, 191
Young C. H., Shirley Y. L., Evans N. J., Rawlings J. M. C., 2003, ApJ, 145, 111

This paper has been typeset from a TEX/LATEX file prepared by the author.